

Physics-constrained Deep Learning of Multi-zone Building Thermal Dynamics

Ján Drgoňa*, Aaron R. Tuor, Vikas Chandan, Draguna L. Vrabie

Pacific Northwest National Laboratory, Richland, WA, USA

Abstract

We present a physics-constrained control-oriented deep learning method for modeling building thermal dynamics. The proposed method is based on the systematic encoding of physics-based prior knowledge into a structured recurrent neural architecture. Specifically, our method incorporates structural priors from traditional physics-based building modeling into the neural network thermal dynamics model structure. Further, we leverage penalty methods to provide inequality constraints, thereby bounding predictions within physically realistic and safe operating ranges. Observing that stable eigenvalues accurately characterize the dissipativeness of the system, we additionally use a constrained matrix parameterization based on the Perron-Frobenius theorem to bound the dominant eigenvalues of the building thermal model parameter matrices. We demonstrate the proposed data-driven modeling approach's effectiveness and physical interpretability on a dataset obtained from a real-world office building with 20 thermal zones. Using only 10 days' measurements for training, we demonstrate generalization over 20 consecutive days, significantly improving the accuracy compared to prior state-of-the-art results reported in the literature.

Keywords: system identification; physics-constrained deep learning; building thermal dynamics; control-oriented modeling

1. Introduction

Energy-efficient buildings are one of the top priorities to sustainably address the global energy demands and reduction of the CO₂ emissions [1, 2]. Advanced control strategies for buildings have been identified as a potential solution with projected energy saving potential up to 28% [3, 4, 5]. The current state of the art approaches in the domain are based on constrained optimal control methods and heavily depend on the mathematical models of the building dynamics [6, 7, 8, 9, 10, 11].

The main bottleneck in the deployment of model predictive control (MPC) in practice is the development of the building thermal dynamics model [12]. In general, the building thermal behavior is characterized by high-dimensional, nonlinear, and often discontinuous dynamics, for which modeling typically requires expertise and development time [13, 14, 15]. Moreover, high computational demands and non-differentiability can easily cast the white-box model as not suitable for efficient gradient-based optimization that is typically used in various applications. Therefore, successful control applications require a trade-off between model accuracy and computational efficiency. Data-driven system identification and controller approximations typically represent more computationally efficient alternatives [16, 17, 18, 19, 20]. However, purely-black box models require a large amount of data and may not generalize well outside the training distribution [21, 22]. On the other hand, identifying accurate and reliable gray-box models remains a challenging task and involves solving difficult non-convex optimization problems [23, 24, 25]. As a consequence, many of the current control-oriented modeling approaches for buildings still rely on crude approximations assuming low-order linear dynamics, which may hamper the overall control performance [26].

In contrast with classical white-, gray-, and black-box modeling approaches, we present a novel data-driven modeling paradigm for building thermal dynamics based on constrained deep learning. We show that we can greatly decrease the required modeling expertise by systematically encoding structural assumptions and constraints while achieving a state of the modeling performance. The proposed neural architecture represents a generic abstraction applicable to an arbitrary building without manual re-design.

1.1. Related Work

Control-oriented building thermal modeling. When properly calibrated, white-box building models can generate highly accurate and reliable results [13]. However, despite significant engineering effort invested in development, due to multiple sources of uncertainty effecting the non-trivial and time-intensive model parameter tuning, white-box models can still result in inaccurate predictions [27]. Moreover, integrating computationally heavy white-box models in real-time optimization routines represents a major challenge and requires significant investment in software development [28, 29].

Due to the higher complexity and cost of white-box models, there is a rising trend towards the use of data-driven methods for predictive control of buildings [30, 31]. However, most of the data-driven approaches in the literature are overly simplified and

*Corresponding author.

Email addresses: jan.drgona@pnnl.gov (Ján Drgoňa), aaron.tuor@pnnl.gov (Aaron R. Tuor), vikas.chandan@kpnnl.gov (Vikas Chandan), draguna.vrabie@pnnl.gov (Draguna L. Vrabie)

mostly applied to single-zone buildings [32]. The most common type of data-driven method is based on linear system identification of reduce order models [33, 34, 35]. Many classical system identification methods typically minimize only 1-step ahead prediction errors. However, as pointed out in [33], optimizing over multi-step ahead prediction errors is much more suitable for predictive control applications. This method is often referred to as MPC relevant identification (MRI) [36, 37], which is based on linear autoregressive models solved via partial least squares (PLS) algorithm. Nonetheless, authors in [26] demonstrated that low-order linear models may not always provide sufficient accuracy and can negatively influence overall MPC performance. On the other hand, machine learning models based on regression trees [18, 38], or neural networks [39, 40, 41] have demonstrated the capability of capturing nonlinear relationships in the building dynamics. However, more complex data-driven models have a tendency to overfit on small datasets [21, 22, 27]. The main drawback of the mentioned black-box models is that they do not incorporate prior knowledge and may provide unreliable predictions by violating underlying physical laws.

Probabilistic semi-physical modeling (PSPM) based on stochastic differential equations [42, 43] falls into the category of gray-box methods requiring prior expert knowledge and manual design of case-specific system dynamics. Resistance-capacitance (RC) networks represent arguably the most popular gray-box modeling method [24, 44]. However, estimating parameters of complex RC networks for large-scale buildings leads to difficult to solve non-convex optimization problems, often requiring manual or heuristic tuning, further increasing the development time and cost [24, 23]. For further discussions and comparisons on different modeling methods used in building control, we refer the reader to the reviews in [16, 22, 45].

Physics-constrained deep learning. Incorporating constraints into neural networks has proven challenging due to non-convexity, a convergence of the learning process, and a requirement for rigorous guarantees of constraint satisfaction [46]. Do to these issues, loss function augmentation via regularization and penalty methods has become the most popular way of imposing constraints in deep learning [47, 48, 49]. Although sacrificing strict bounds, it has been shown that soft constrained penalty methods work well in practice and often outperform methods based on hard constraints, such as barrier methods [50, 51]. Alternatively, architecture design methods focus on incorporating strong inductive biases inspired by physics, for instance, architectures respecting energy conservation laws. Examples of such architecture are linear operator constraints [52], Hamiltonian [53] or Lagrangian [54] neural networks. From an architecture perspective, the work we present here is inspired by a family of neural state-space models (SSM) [55, 56, 57, 58, 59], representing structurally modified vanilla RNNs tailored for the modeling of dynamical systems for control.

In recent years several authors interpreted deep neural networks through the optics of differential equations [60, 61, 62]. This new line of research opened the doors for a more rigorous analysis of the neural dynamics. For instance, authors in [63] linked the vanishing and exploding gradient problems in recurrent neural networks (RNN) with the eigenvalues and stability of neural networks. Others proposed new architectures with stability guarantees based on constraining the eigenvalues of neural network layers [64, 65]. In this paper, we leverage the eigenvalue constraints method based on Perron-Frobenius theorem [66] interpreted through the perspective of building physics. Additionally, we use penalty methods to constrain the learned dynamics' phase space within physically realistic bounds.

1.2. Contributions

This paper shows how to train physics-constrained recurrent neural dynamics models tailored to efficiently learn the building's thermal dynamics in an end-to-end fashion, with physically coherent generalization, from small datasets. This work is a conceptual extension of author's previous work on using constrained-deep learning models for system identification and control of small-scale building thermal dynamics model [66, 67]. We empirically demonstrate the accuracy and generalization of the proposed physics-constrained neural architectures using only 10 days of training data from a real-world office building with 20 thermal zones. Compared to their unstructured and unconstrained counterparts, the presented constrained recurrent neural models show a 15% reduction in error. We introduce several novel key features of the presented modeling approach resulting in increased data-efficiency, accuracy, generalization, and systematic constraint handling compared to unconstrained deep learning models:

1. Encoding the underlying graph structure of the building dynamics as block-structured recurrent neural dynamics models.
2. Eigenvalue constraints based on Perron-Frobenius theorem yielding guarantees on stability and dissipativity of learned dynamics.
3. Penalty methods for imposing inequality constraints representing physically meaningful boundary conditions of learned dynamics.
4. Multi-step multi-term loss function for learning long-term and physically coherent dynamical models.
5. Physical interpretation of eigenvalue analysis of neural network weights for inspection of the desired dynamical properties of the learned models.

To the author's best knowledge, this is the first combined use of structured recurrent neural architectures with physics-inspired constraints applied to a real-world building thermal dynamics modeling problem.

2. Methods

2.1. Building Thermal Dynamics

When developing predictive models for control purposes, one has to balance model complexity, robustness, and accuracy. The typical building envelope dynamics is represented by a model with a graph structure shown in Fig. 1a. Mathematically, the thermal building model is given as the following difference equation with nonlinear input and disturbance dynamics:

$$\mathbf{x}_{t+1} = A\mathbf{x}_t + B\mathbf{q}_t + f_d(\mathbf{d}_t), \quad (1a)$$

$$\mathbf{y}_t = C\mathbf{x}_t, \quad (1b)$$

$$\mathbf{q}_t = \dot{\mathbf{m}}_t cp \Delta \mathbf{T}_t, \quad (1c)$$

where \mathbf{x}_t and \mathbf{y}_t represent the values of the states (envelope temperatures), and measurements (zone temperatures) at time t , respectively. Disturbances \mathbf{d}_t represent the influence of weather and occupancy behavior. Heat flows delivered to the building \mathbf{q}_t are represented by (1c) heat flow equation as a product of mass flows $\dot{\mathbf{m}}_t$, difference of the supply and return temperatures $\Delta \mathbf{T}_t$, and the specific heat capacity constant cp . Tab. 1 summarizes the variables used for data-driven modeling of the underlying building thermal dynamics.

Table 1: Abstract variable notation of the data-driven neural model of the building thermal dynamics.

Notation	Neural model	Building physics	Units
\mathbf{x}	hidden states	envelope temperatures, heat flows	[K, W]
\mathbf{y}	outputs	room operative temperatures	[K]
\mathbf{u}	control actions	mass flows, supply temperatures	[kg/s, K]
\mathbf{d}	disturbances	ambient temperature	[K]
\mathbf{s}	slack variables	violations of boundary conditions	[K, W]

When the model is built with perfect knowledge from first principles, it is physically interpretable. For instance, the A matrix represents 1-D heat transfer between the spatially discretized system states. B matrix defines the temperature increments caused by the convective heat flow (1c) generated by the HVAC system, while f_d captures highly nonlinear thermal dynamics caused by the weather conditions or internal heat gains generated by the occupancy. However, every building represents a unique system with different operational conditions. Therefore, obtaining the parameters of the difference equations (1) from first principles is a time-consuming, impractical task.

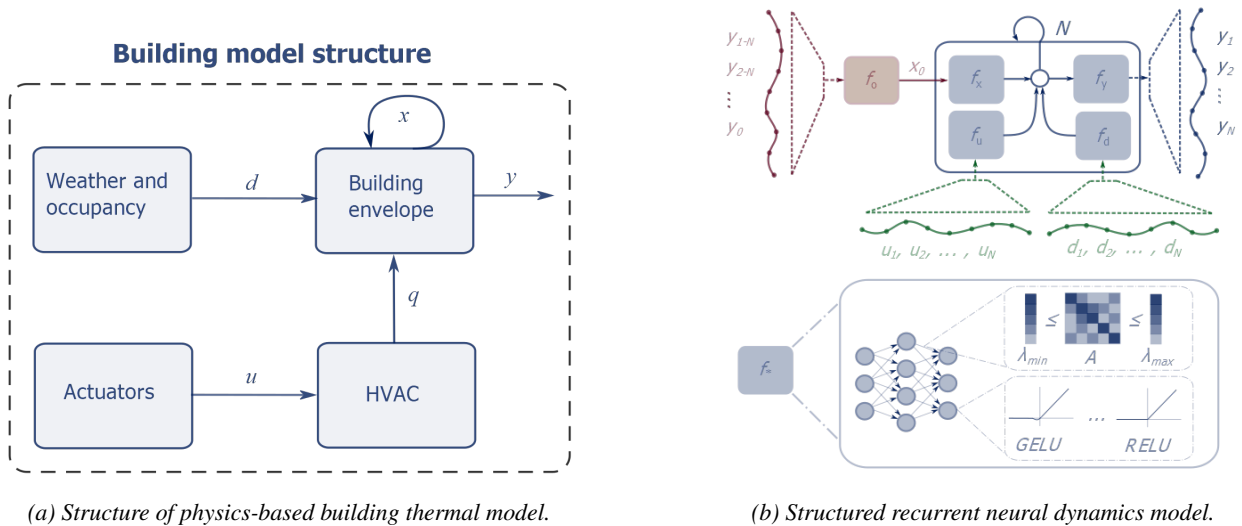


Figure 1: Generic structure of physics-inspired recurrent neural dynamics model architecture. Weights of individual neural blocks f_* are parametrized by linear maps with constrained eigenvalues, while component outputs are subject to penalty constraints parametrized by common activation functions.

2.2. Unstructured Recurrent Neural Dynamics Model

The white-box building model (1) is represented by a partially observable discrete ordinary differential equation (ODE) describing the evolution of the system's state over time. Assuming zero prior knowledge about the model structure can translate

this discrete ODE into an unstructured state-space model (SSM):

$$\mathbf{x}_{t+1} = f(\mathbf{x}_t, \mathbf{u}_t, \mathbf{d}_t) \quad (2a)$$

$$\mathbf{y}_t = f_y(\mathbf{x}_t) \quad (2b)$$

$$\mathbf{x}_0 = f_o([\mathbf{y}_{1-N}; \dots; \mathbf{y}_0]) \quad (2c)$$

Where f represents the main system dynamics, while f_y defines the output mapping. We are using neural networks to encode the mappings f and f_y and we refer to this model as unstructured recurrent neural dynamical model.

2.3. Structured Recurrent Neural Dynamics Model

The systems such as (1) with linear state dynamics and nonlinear input dynamics are formally referred to as block-structured state-space models. Conveniently, we can assume this generic structure to be invariant across building types and sizes. Fig. 1b shows the overall architecture of the physics-inspired neural dynamics model for partially observable systems. To further promote physically coherent behavior, the neural component blocks f_* are parametrized by linear maps with constrained eigenvalues and regularized with penalty functions, as explained in the following sections. The block-structured recurrent neural dynamics model is defined as:

$$\mathbf{x}_{t+1} = f_x(\mathbf{x}_t) + f_u(\mathbf{u}_t) + f_d(\mathbf{d}_t) \quad (3a)$$

$$\mathbf{y}_t = f_y(\mathbf{x}_t) \quad (3b)$$

$$\mathbf{x}_0 = f_o([\mathbf{y}_{1-N}; \dots; \mathbf{y}_0]) \quad (3c)$$

Here f_x , f_u , and f_d represent decoupled neural components of the overall system model, corresponding to state, input, and disturbance dynamics, respectively. We assume only partially observable systems where states \mathbf{x} represent latent dynamics. As a consequence, we need to use state observer given as additional neural component, f_o , encoding a past N -step window of observations \mathbf{y} onto initial state conditions \mathbf{x}_0 . During training, the model is unrolled and trained on an N -step ahead prediction window. The main advantage of the block nonlinear over unstructured black-box state-space model lies in its structure. The decoupling allows us to leverage prior knowledge for imposing structural assumptions and constraints onto individual blocks of the model. Please note the structural similarity between the proposed neural model (3) and difference equation (1).

2.4. Eigenvalue Constraints

An important physics insight is that building thermal dynamics represents a dissipative system with stable eigenvalues. The system's dissipativity is physically interpreted as heat losses of the building envelope, which are influenced by numerous factors such as building topology, material properties, insulation levels, or window-to-wall ratio. These parameters determine the overall heat transfer coefficient of the building, called U-values, where smaller U-values mean better insulation. The problem is that obtaining accurate information about the parameters required for estimation of the U-values from technical sheets is time consuming and tedious task. From a dynamical perspective, U-values can be loosely related to the system eigenvalues. This inspired us to enforce physically reasonable constraints on the eigenvalues of a model's weight matrices.

We leverage the method based on the Perron-Frobenius theorem, which states that the row-wise minimum and maximum of any positive square matrix defines its dominant eigenvalue's lower and upper bound, respectively. Guided by this theorem, we can construct a state transition matrix $\tilde{\mathbf{A}}$ with bounded eigenvalues:

$$\mathbf{M} = \lambda_{\max} - (\lambda_{\max} - \lambda_{\min})\sigma(\mathbf{M}') \quad (4a)$$

$$\tilde{\mathbf{A}}_{i,j} = \frac{\exp(\mathbf{A}'_{ij})}{\sum_{k=1}^{n_x} \exp(\mathbf{A}'_{ik})} \mathbf{M}_{i,j} \quad (4b)$$

We introduce a matrix \mathbf{M} which models damping parameterized by the matrix $\mathbf{M}' \in \mathbb{R}^{n_x \times n_x}$. We apply a row-wise softmax to another parameter matrix $\mathbf{A}' \in \mathbb{R}^{n_x \times n_x}$, then elementwise multiply by \mathbf{M} to obtain our state transition matrix $\tilde{\mathbf{A}}$ with eigenvalues lower and upper bounds λ_{\min} and λ_{\max} . Further in the text we refer to this factorization as `pf` weight. In case study, we compare the `pf` factorization with standard unconstrained version referred to as `linear` weight.

2.5. Inequality Constraints via Penalty Methods

Using an optimization strategy known as the penalty method, we can add further constraints to our model such that its variables remain within physically realistic bounds. We enforce this property by applying inequality constraints via penalty functions $p(\mathbf{y})$ for each time step t :

$$p(\mathbf{y}_t, \bar{\mathbf{y}}_t) : \mathbf{y}_t - \mathbf{s}_t^{\bar{y}} \leq \bar{\mathbf{y}}_t \cong \mathbf{s}_t^{\bar{y}} = \max(0, \mathbf{y}_t - \bar{\mathbf{y}}_t) \quad (5a)$$

$$p(\mathbf{y}_t, \underline{\mathbf{y}}_t) : \underline{\mathbf{y}}_t \leq \mathbf{y}_t + \mathbf{s}_t^{\underline{y}} \cong \mathbf{s}_t^{\underline{y}} = \max(0, -\mathbf{y}_t + \underline{\mathbf{y}}_t) \quad (5b)$$

The constraints lower and upper bounds are given as \underline{y}_k and \bar{y}_k , respectively. The slack variables s_k^y and $s_k^{\bar{y}}$ indicate the magnitude to which each constraint is violated, and we penalize them heavily in the optimization objective by a large weight on these additional terms in the loss function. These constraints can be straightforwardly implemented using standard `RELU` functions (see right-hand sides of (5)) and included as auxiliary weighted terms in the loss function.

To understand how the penalties enforce the output value constraints, let's focus on the upper-bound penalty (5a). Notice that if the difference between the output \mathbf{y}_t and its upper bound \bar{y}_t is positive, then the output value is exceeding the bound, resulting in a non-zero value of the slack variable $s_t^{\bar{y}}$. Otherwise, if the result is negative, the output must be within bounds, and the constraint is satisfied indicated by the zero-valued slack variable $s_t^{\bar{y}}$. The same intuition can be applied to the lower-bound constraint (5b). Please note that penalty-based inequality constraints can be imposed on arbitrary model variables based on their assumed or known physical limits.

2.6. Multi-step Multi-term Loss Function

We optimize the following loss function augmented with regularization and penalty terms to train the recurrent neural model (3) unrolled over N steps:

$$\mathcal{L}_{\text{MSE}}(\mathcal{Y}^{\text{ref}}, \mathcal{Y}|\Theta) = \frac{1}{N} \sum_{t=1}^N \|\mathbf{y}_t^{\text{ref}} - \mathbf{y}_t\|_2^2 + Q_{\text{dx}} \|\mathbf{x}_t - \mathbf{x}_{t-1}\|_2^2 + Q_{\text{ineq}}^y \|s_t^y\|_2^2 + Q_{\text{ineq}}^u \|s_t^{f_u}\|_2^2 + Q_{\text{ineq}}^d \|s_t^{f_d}\|_2^2 \quad (6)$$

The first term of the loss function computes the mean squared error between predicted \mathbf{y} and observed outputs \mathbf{y}^{ref} over N time steps and represents our primary objective. Following similar arguments as in the case of MRI method [33], optimizing over N -step prediction window improves the overall accuracy and generalization of the learned system dynamics model. The term $\mathbf{x}_t - \mathbf{x}_{t-1}$ represents state difference penalty promoting learning of smoother and physically more plausible state trajectories. The violations of the inequality constraints defining the boundary conditions of outputs \mathbf{y} , are penalized by incorporating weighted slack variables s^y . Thanks to the block-structured dynamics, we can constrain the dynamical contribution of inputs f_u and disturbances f_d towards the overall dynamics via two additional terms in the loss function. This allows us to limit the effect of the external factors to be bounded within physically plausible ranges. For instance, it is not physically realistic that 1 K change in the ambient temperature would cause a 2 K change in indoor temperature in a single time step.

3. Experimental Case Study

The objective is to develop a control-oriented model of the thermal dynamics of a commercial office building, given only a limited amount of time series measurement data.

3.1. Real-world Building Dataset and Experimental Setup

Real-world Building Dataset. The building used in this study is a commercial building in Richland, WA described in [68]. Heating and cooling are provided by a variable air volume (VAV) system served by 4 air handling units (AHUs) serving 24 VAV boxes (zones). Each VAV box is equipped with a hot water reheat coil. A boiler, fed by natural gas, supplies hot water to the reheat coils and AHU coils. Chilled water is supplied by a central chiller plant.

Data from specific sensors for the above-mentioned buildings is stored in a database, which communicates with the building management system (BMS) and polls data for these sensors at a time resolution of 1 minute. A total of more than 600 sensors report data corresponding to measurements such as supply and return temperatures of air and water, air, hot water and cold water flow rates, energy and power consumption, set-points for the underlying control systems, occupancy status in zones, and outside air temperature. Data was cleaned and pre-processed according to the methodology described in [68]. The same dataset was used in [68] to model the building's power consumption and zone temperatures using RNN model with LSTM architecture. The authors have been able to achieve high prediction accuracy on a single step ahead prediction compared to other standard machine learning models such as linear regression, support vector regression, and random forests. However, due to the purely black-box nature and 1-step ahead loss function, the model in [68] does not explicitly guarantee physical constraints and is not suitable for long-term predictions of the building's thermal behavior. This case study demonstrates improved accuracy, generalization, long-term prediction capabilities, and physically coherent and interpretable dynamic behavior of the learned dynamical model with 20 thermal zones. Hence, considering a model with higher complexity compared to the 2-zone model presented in [68].

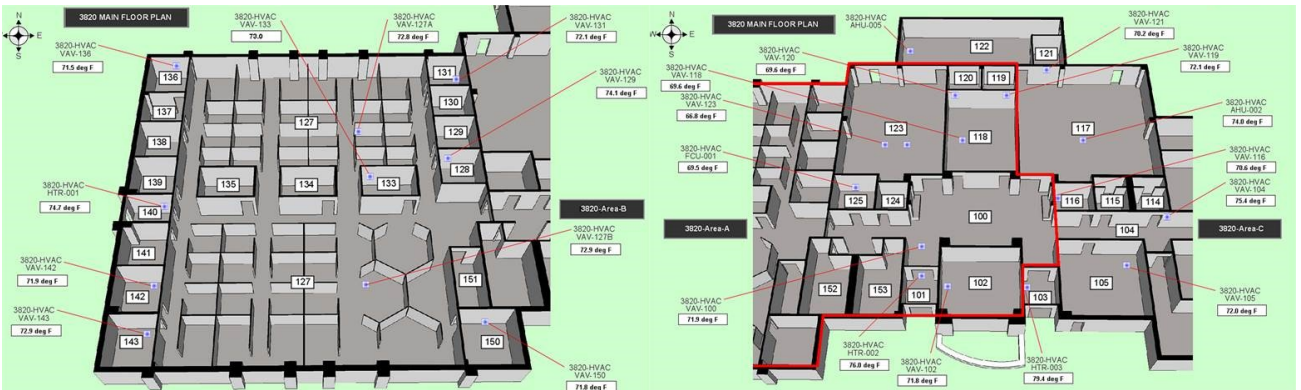
The time series dataset D with datapoints relevant for system identification of thermal dynamics is given in the form of tuples with input, disturbance, and output variables, respectively.

$$D = \{(\mathbf{u}_t^{(i)}, \mathbf{d}_t^{(i)}, \mathbf{y}_t^{(i)}), (\mathbf{u}_{t+\Delta}^{(i)}, \mathbf{d}_{t+\Delta}^{(i)}, \mathbf{y}_{t+\Delta}^{(i)}), \dots, (\mathbf{u}_{t+N\Delta}^{(i)}, \mathbf{d}_{t+N\Delta}^{(i)}, \mathbf{y}_{t+N\Delta}^{(i)})\}, \quad (7)$$

where $i = \mathbb{N}_1^n$ represents index of n different batches of time series trajectories with N -step time horizon length. The data is sampled with fixed sampling time $\Delta = 15$ min. We have in total $n_y = 20$ output variables corresponding to zone temperatures,



(a) Building's facade.



(b) Building's zone layout.

Figure 2: Office building of interest.

$n_u = 40$ input variables representing HVAC temperatures and mass flows, and $n_d = 1$ disturbance variable representing ambient temperature forecast. Before training, we use `min-max` normalization to scale all variables between $[0, 1]$. The dataset consists of 30 days, which corresponds to only 2880 datapoints. We group the dataset into evenly split training, validation, and test sets, 960 data points each. We select the best performing models on the open-loop MSE for the development set and report results on the test set.

Experimental Setup. We implement the presented model architectures using Pytorch [69], and train with randomly initialized weights using the Adam optimizer [70] with a learning rate of 0.003, and 5,000 gradient descent updates. We select the best performing model on the development set from a directed hyperparameter search. All neural network blocks are designed with GELU activation functions [71]. The state estimator is encoded with a fully connected neural network, while individual neural blocks f_* are represented either by standard multilayer perceptron (MLP), recurrent neural network (RNN), or residual neural network (ResNet), respectively, each with 2 layers and 80 nodes. We range the prediction horizon as powers of two 2^n with $n = 3, \dots, 6$, which corresponds to 2 up to 16 hour prediction window. The relative weights of the multi-term loss function for constrained models are $Q_{dx} = 0.2$, $Q_{ineq}^y = 1.0$, $Q_{ineq}^u = 0.2$, and $Q_{ineq}^d = 0.2$. We set $\lambda_{min} = 0.8$ and $\lambda_{max} = 1.0$ for stability and low dissipativity of learned dynamics when using eigenvalue constraints.

3.2. Results and Analysis

This section assesses the open-loop and N -step simulation performance of trained recurrent neural dynamics models with and without structure and constraints, respectively. We systematically compare and analyze the added value of the block structure, penalty, and eigenvalue constraints, where Tab. 2 summarizes the best performance of the modeling variants. Moreover, we discuss the interpretability of the proposed data-driven models through the optics of building physics.

Table 2: Test set MSE of best-performing structured, unstructured, constrained and unconstrained models, respectively.

Structure	Constrained	Weights	N	N -step [K]	Open-loop [K]
Structured	Y	Linear	64	0.4811	0.4884
	N	Perron-Frobenius	16	0.4720	0.5043
Unstructured	Y	Linear	64	0.5380	0.5446
	N	Linear	16	0.5266	0.5596

Best performing model. As reported in Tab. 2, we achieve the best performance with constrained and structured recurrent neural model (3). The best model scores 0.0052, 0.0091, and 0.0143, on normalized open-loop MSE evaluated on the test, dev, and train set, respectively. From a physical perspective, the denormalized open-loop MSE corresponds to roughly 0.18K, 0.31K, and 0.49K errors per output, respectively. This demonstrates the ability to generalize the dynamics over the period of 30 days, given only 10 days of training data. In comparison, the state of the art gray-box and black-box system identification methods trained on a similar amount of data reports open-loop MSE greater than 1.0K [23, 72, 73]. Hence our results show more than 100% improvement against state of the art. However, a more rigorous comparison needs to be performed to compare the accuracy with standard gray-box methods using the same datasets. For visual assessment, Fig. 3 shows normalized open-loop simulation trajectories of best performing structured dynamics model on the train, dev, and test set, represented by gray zones, respectively.

Effect of prediction horizon and penalty constraints. Fig. 4 shows test set performance with open-loop MSE and N -step ahead MSE losses for structured and constrained model variants trained with increasing prediction horizon N . As expected, Fig. 4b shows that N -step MSE rises with a longer prediction horizon in the training loss function because learning long-term predictions is generally a more difficult task. Tab. 2 reports larger MSE gaps between N -step and open-loop loss for smaller prediction horizon $N = 16$. On the other hand, larger horizon $N = 64$ minimizes the gap between N -step loss function and open-loop performance, hence providing a more accurate assessment of the desired performance measure. Also, as shown in Fig. 4a, longer prediction horizon tends to improve the overall open-loop simulation performance of all constrained models. The same does not hold for unconstrained models for which the performance starts to deteriorate with a horizon longer than 16. This indicates that including penalty constraints in the training loss function helps to improve the model accuracy over longer prediction horizons. The intuition here is simple; by confining the system outputs into a physically meaningful subspace, the model is less likely to learn diverging long-term trajectories.

Effect of physics-inspired structure. Fig. 4 demonstrates that adding building-physics inspired structure into the neural state-space model undeniably improves both open-loop and N -step MSE. Results in Tab. 2 confirm that both constraints and structure have a positive influence on the open-loop performance of trained models, while structure being a more significant modeling assumption. Applying both structure and constraints yields a 15% reduction in error against unstructured and unconstrained neural state-space model counterparts. By decoupling the state, control action, and disturbance dynamics into separate blocks modeled by

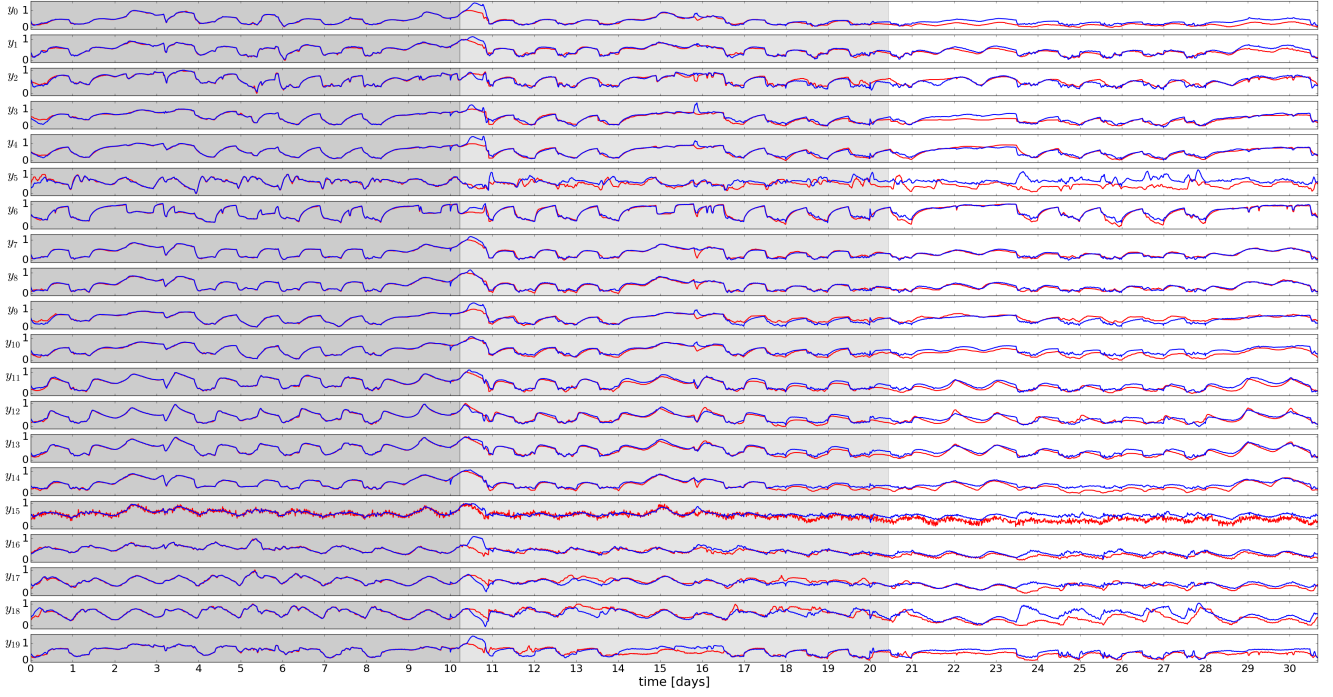


Figure 3: Open-loop trajectories of the learned (blue) and ground truth (red) multi-zone building thermal dynamics.

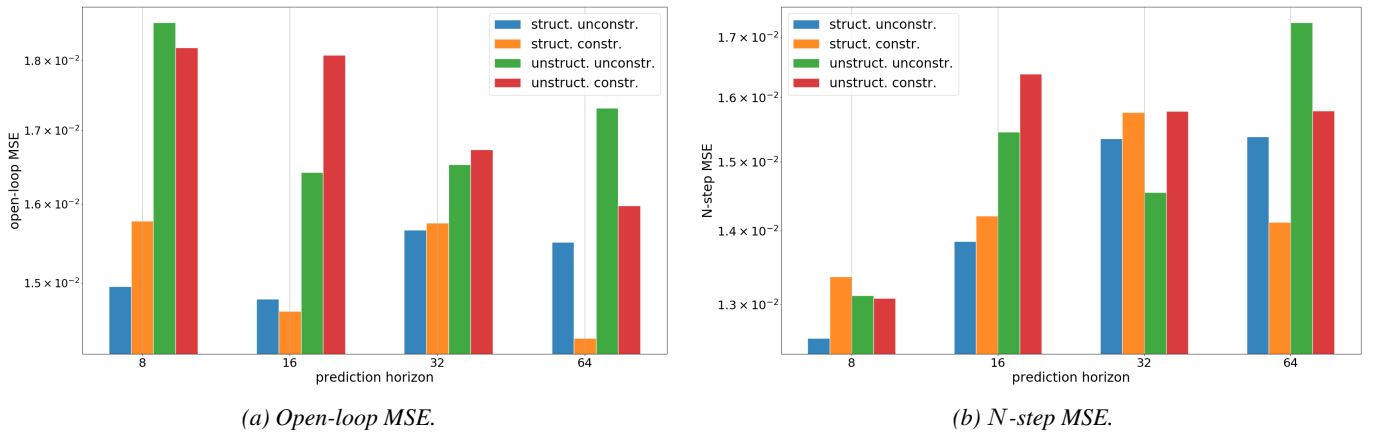


Figure 4: Effect of penalty constraints on open-loop and N -step ahead MSE evaluated on a test set using structured and unstructured models, with increasing training prediction horizon N .

neural networks, we prevent the model from learning lumped dynamics behavior. Each block can now learn different nonlinear transformations, which can be independently interpreted as structural heat transfer dynamics for states f_x , HVAC dynamics for inputs f_u , and weather and occupancy thermal dynamics for disturbance signals f_d .

Effect of neural blocks architecture. Fig. 5 shows the effect on open-loop and N -step MSE of using different neural architectures for representing the individual blocks of structured and unstructured neural state-space models, respectively. We focus our analysis on best-case open-loop performance displayed in Fig. 6a. Please note the y-axis is in the logarithmic scale. Surprisingly, models with ResNet architectures are less accurate than best performing RNN or MLP across all prediction horizons and deteriorate fast with increasing prediction horizon. The cause of ResNets' poor performance is hard to estimate at this point, and more in-depth analysis needs to be performed in the future. On the other hand, the performance of models with both RNN and MLP blocks is comparable and scales well also with larger horizons. While models with RNN blocks tend to perform better for shorter horizons, models with MLP architecture score better for the largest time horizon of 64 steps. This might be linked with well known RNN issues, such as vanishing, and exploding gradient problems causing difficulties when learning long-term dependencies [74, 75].

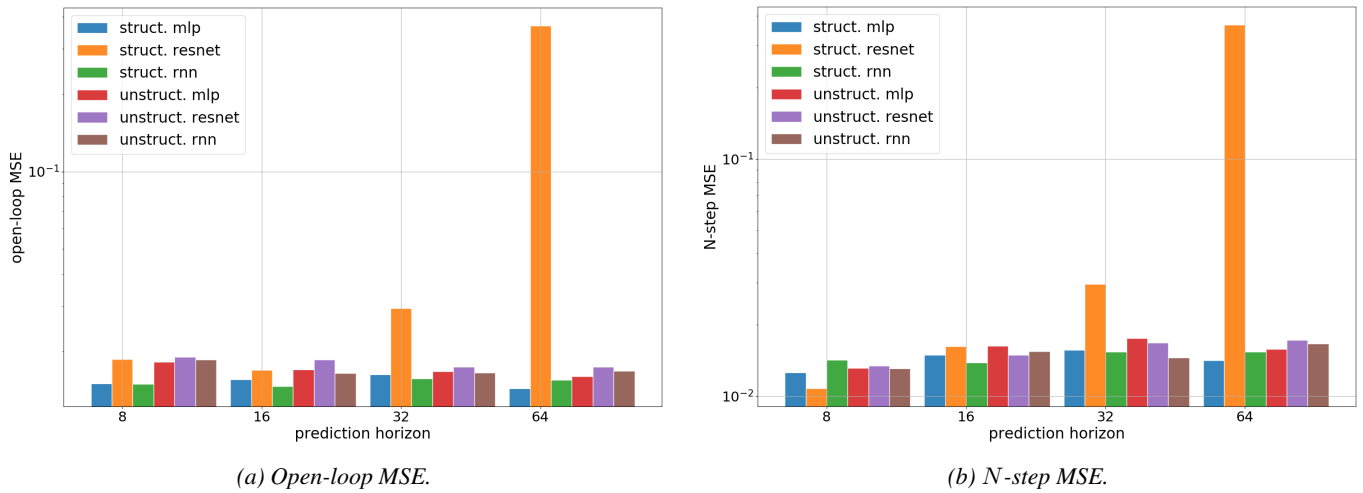


Figure 5: Effect of neural blocks architecture on open-loop and N -step ahead MSE evaluated on a test set using structured and unstructured models, with increasing training prediction horizon N .

Effect of weight's eigenvalue constraints. Fig. 6 shows test set performance with open-loop MSE and N -step ahead MSE losses for structured and unstructured model variants with and without eigenvalue constraints via pf factorization of weights. Due to restrictive nature of the pf factorization, in Fig. 6b we observe larger increase in N -step MSE compared to unconstrained linear weights for most of the cases. However, as shown in in Fig. 6a, the eigenvalue constraints improve the performance of the structured models for shorter prediction horizons, as a consequence of the imposed inductive bias towards learning dissipative heat transfer dynamics. On the other hand, unstructured models do not benefit from using pf factorization at all. The reason is that imposed eigenvalue constraints are inspired by the building envelope dynamics exclusively modeled with f_x map of structured models (3). In contrast, unstructured models (2) learn lumped envelope, HVAC, and disturbance dynamics, hence they fail to benefit from any block-specific priors.

3.3. Eigenvalue Analysis and Physical Interpretability

Fig. 7 shows concatenated eigenvalues in the complex plane for weights of the state transition maps f_x and f of learned structured (3) and unstructured (2) recurrent neural dynamics models, respectively. Besides structure Fig. 7 compares the effect of eigenvalue constraints using Perron-Frobenius (pf) factorization of the system dynamics weights. Please note that we plot only eigenvalues of the neural network's weights. Hence the dynamic effects of the activation functions are omitted in this analysis. However, all our neural network blocks are designed with GELU activation functions, which represent contractive maps with strictly stable eigenvalues. Therefore, based on the argument of the composition of stable functions, the global stability of the learned dynamics is not compromised.

Fig. 7a shows the effect of proposed eigenvalue constraints pf factorization, and verifies that the dominant eigenvalue remains within prescribed bounds $\lambda_{\min} = 0.8$ and $\lambda_{\max} = 1.0$. Hence the dissipativeness of the learned dynamics is hard constrained within physically realistic values when using pf factorization. Another interesting observation is that there are only two dominant dynamical modes with eigenvalues larger than 0.8, one per each layer of f_x . While the rest of the eigenvalues fall within 0.05 radius, hence representing less significant dynamic modes [76, 77]. This indicates a possibility to obtain lower-order representations of the underlying higher-order nonlinear system, a property useful for real-time optimal control applications.

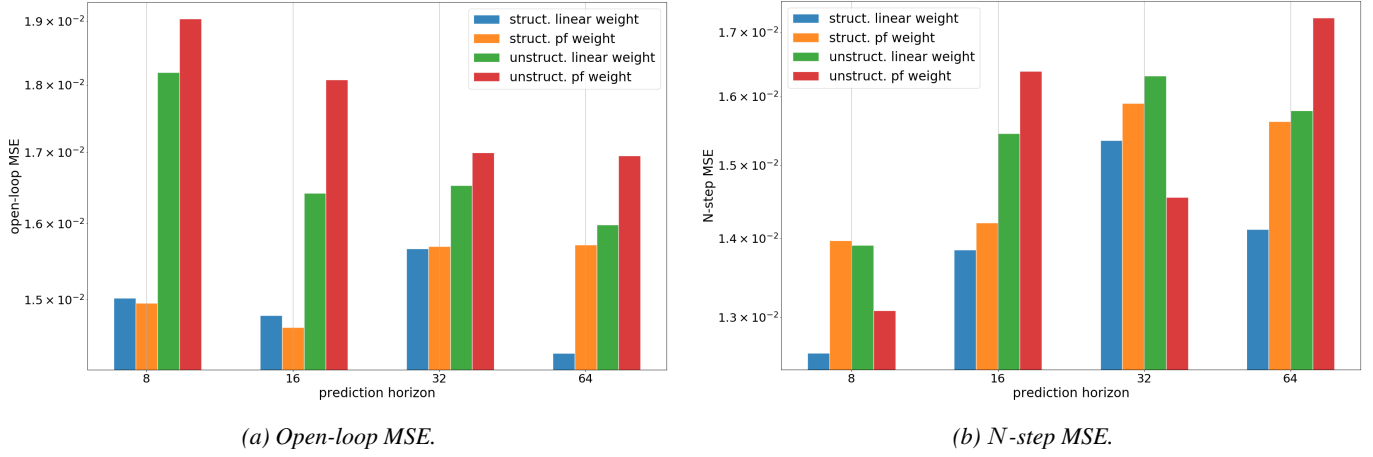
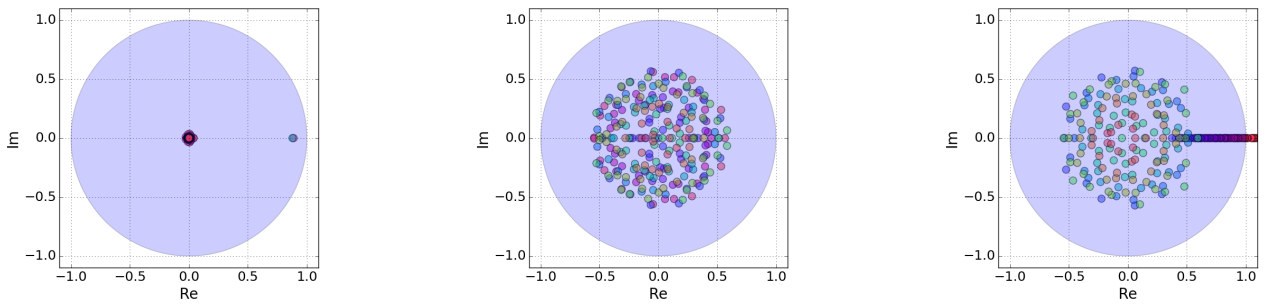


Figure 6: Effect of eigenvalue constraints via pE factorization on open-loop and N -step ahead MSE evaluated on a test set using structured and unstructured models, with increasing training prediction horizon N .



(a) Eigenvalues of pE factorized weights of structured model (3) dynamics f_x .

(b) Eigenvalues of unconstrained weights of structured model (3) dynamics f_x .

(c) Eigenvalues of unconstrained weights of unstructured model (2) dynamics f .

Figure 7: Eigenvalue plots of the weights of system dynamics maps f_x , and f of learned structured and unstructured dynamical models, respectively. Blue circles represent stable regions.

In contrast, as displayed in Fig. 7a and Fig. 7c, the eigenvalues of standard unconstrained weights for both structured and unstructured models are more dispersed with larger imaginary parts. The imaginary parts indicate oscillatory modes of the autonomous state dynamics f_x and f , respectively. However, in the case of building thermal dynamics, the periodicity of the dynamics is caused by external factors such as weather and occupancy schedules. From this perspective, the structured models using pF factorization of the weights, are closer to the physically realistic parameterization of the system dynamics. Additionally, not using eigenvalue constraints may result in learning unstable weights. Fig. 7c displays an example where the unstructured learned model does not guarantee the satisfaction of physically realistic dissipativeness property.

4. Conclusions

Control-oriented system dynamic models are indispensable parts of most advanced building control strategies, such as model predictive control. Consequently, reliable data-driven modeling methods that are cost-effective in terms of computational demands, data collection, and domain expertise have the potential to revolutionize the field of energy-efficient building operations through the wide-scale acquisition of building specific, scalable, and accurate prediction models. Here we presented a constrained deep learning method for sample-efficient and physics-consistent data-driven modeling of building thermal dynamics. Our approach does not require the large time investments by domain experts and extensive computational resources demanded by physics-based emulator models. Based on only 10 days' measurements, we significantly improve on prior state-of-the-art results for a modeling task using a real-world large scale office building dataset. This improvement in model predictions is attributed to our contributions of structural assumptions, eigenvalue constraints imposed on weights, and penalty methods imposed on the outputs of a deep recurrent neural network model. We systematically analyze the added value of the proposed structural assumptions and constraints in comparison with their unstructured and unconstrained model counterparts. Additionally, we assess the interpretability and level of physical realism of the learned system dynamics by connecting the neural weights' eigenvalue analysis with known dynamical properties of buildings. The modeling results using a real-world dataset obtained from a large-scale office building demonstrate the accuracy, data-efficiency, and interpretability of the proposed method. A potential limitation of the presented approach is the restrictiveness of the used constraints, where wrong initial guess of the eigenvalue and penalty constraints bounds may lead to decreased accuracy of the learned model. Hence, some level of engineering insight is required to properly use the presented methodology for modeling building's thermal dynamics. Future work includes a systematic comparison against physics-based emulator models and other standard data-driven methods. Authors also plan to use the method as part of advanced predictive control strategies for energy-efficient operations in real-world buildings.

ACKNOWLEDGEMENT

This work was funded by the Physics Informed Machine Learning (PIML) investment at the Pacific Northwest National Laboratory (PNNL). This work emerged from the IBPSA Project 1, an international project conducted under the umbrella of the International Building Performance Simulation Association (IBPSA).

References

- [1] David Rolnick, Priya L. Donti, Lynn H. Kaack, Kelly Kochanski, Alexandre Lacoste, Kris Sankaran, Andrew Slavin Ross, Nikola Milojevic-Dupont, Natasha Jaques, Anna Waldman-Brown, Alexandra Luccioni, Tegan Maharaj, Evan D. Sherwin, S. Karthik Mukkavilli, Konrad P. Kording, Carla Gomes, Andrew Y. Ng, Demis Hassabis, John C. Platt, Felix Creutzig, Jennifer Chayes, and Yoshua Bengio. Tackling climate change with machine learning. *CoRR*, abs/1906.05433, 2019.
- [2] IEA International Energy Agency and International Partnership for Energy Efficiency Cooperation. Building energy performance metrics - supporting energy efficiency progress in major economies. Technical report, IEA Publications, 2015.
- [3] K. W. Roth, D. Westphalen, J. Dieckmann, S. D. Hamilton, and W. Goetzler. Energy Consumption Characteristics of Commercial Building HVAC Systems - Volume III: Energy Savings Potential. Technical report, 2002.
- [4] D. Gyalistras, M. Gwerder, F. Schildbach, C.N. Jones, M. Morari, B. Lehmann, K. Wirth, and V. Stauch. Analysis of Energy Savings Potentials for Integrated Room Automation. In *Clima - RHEVA World Congress*, Antalya, Turkey, May 2010.
- [5] Ján Drgoňa, Javier Arroyo, Iago Cupeiro Figueroa, David Blum, Krzysztof Arendt, Donghun Kim, Enric Perarnau Ollé, Juraj Oravec, Michael Wetter, Draguna L. Vrabie, and Lieve Helsen. All you need to know about model predictive control for buildings. *Annual Reviews in Control*, 2020.
- [6] Jan Široký, Frauke Oldewurtel, Jiří Cigler, and Samuel Prívvara. Experimental analysis of model predictive control for an energy efficient building heating system. *Applied Energy*, 88(9):3079–3087, 2011.

- [7] Y. Ma, F. Borrelli, B. Hancey, B. Coffey, S. Bengea, and P. Haves. Model predictive control for the operation of building cooling systems. *IEEE Transactions on Control Systems Technology*, 20(3):796–803, 2012.
- [8] Mehdi Maasoumy, Barzin Moridian, Meysam Razmara, Mahdi Shahbakhti, and Alberto Sangiovanni-Vincentelli. Online simultaneous state estimation and parameter adaptation for building predictive control. In *ASME 2013 Dynamic Systems and Control Conference*, pages V002T23A006–V002T23A006. American Society of Mechanical Engineers, 2013.
- [9] Vikas Chandan and Andrew G Alleyne. Decentralized predictive thermal control for buildings. *Journal of Process Control*, 24(6):820–835, 2014.
- [10] Simone Baldi, Shuai Yuan, Petr Endel, and Ondrej Holub. Dual estimation: Constructing building energy models from data sampled at low rate. *Applied Energy*, 169:81–92, 2016.
- [11] Ján Drgoňa, Damien Picard, and Lieve Helsen. Cloud-based implementation of white-box model predictive control for a GEOTABS office building: A field test demonstration. *Journal of Process Control*, 88:63 – 77, 2020.
- [12] J. Cigler, D. Gyalistras, J. Široký, V. Tiet, and L. Ferkl. Beyond Theory: the Challenge of Implementing Model Predictive Control in Buildings. In *Proceedings of 11th Rehva World Congress, Clima, Prague, Czech Republic*, 2013.
- [13] F. Jorissen, G. Reynders, R. Baetens, D. Picard, D. Saelens, and L. Helsen. Implementation and verification of the IDEAS building energy simulation library. *Journal of Building Performance Simulation*, 11(6):669–688, 2018.
- [14] M. Wetter, W. Zuo, T. Nouidui, and X. Pang. Modelica buildings library. *Journal of Building Performance Simulation*, 7(4):253–270, 2014.
- [15] Hao Gao, Christian Koch, and Yupeng Wu. Building information modelling based building energy modelling: A review. *Applied Energy*, 238:320 – 343, 2019.
- [16] Nadia D. Roman, Facundo Bre, Victor D. Fachinotti, and Roberto Lamberts. Application and characterization of metamodels based on artificial neural networks for building performance simulation: A systematic review. *Energy and Buildings*, 217:109972, 2020.
- [17] Yuna Zhang, Zheng O’Neill, Bing Dong, and Godfried Augenbroe. Comparisons of inverse modeling approaches for predicting building energy performance. *Building and Environment*, 86:177 – 190, 2015.
- [18] Francesco Smarra, Achin Jain, Tullio de Rubeis, Dario Ambrosini, Alessandro D’Innocenzo, and Rahul Mangharam. Data-driven model predictive control using random forests for building energy optimization and climate control. *Applied Energy*, 226:1252 – 1272, 2018.
- [19] L. Ferkl and J. Široký. Ceiling radiant cooling: Comparison of armax and subspace identification modelling methods. *Building and Environment*, 45(1):205 – 212, 2010.
- [20] Ján Drgoňa, Damien Picard, Michal Kvasnica, and Lieve Helsen. Approximate model predictive building control via machine learning. *Applied Energy*, 218:199 – 216, 2018.
- [21] Abdul Afram and Farrokh Janabi-Sharifi. Review of modeling methods for HVAC systems. *Applied Thermal Engineering*, 67(1):507 – 519, 2014.
- [22] Zakia Afroz, GM Shafullah, Tania Urmees, and Gary Higgins. Modeling techniques used in building HVAC control systems: A review. *Renewable and Sustainable Energy Reviews*, 2018.
- [23] Javier Arroyo, Fred Spiessens, and Lieve Helsen. Identification of multi-zone grey-box building models for use in model predictive control. *Journal of Building Performance Simulation*, 13(4):472–486, 2020.
- [24] Krzysztof Arendt, Muhyiddine Jradi, Michael Wetter, and Christian Veje. ModestPy: An Open-Source Python Tool for Parameter Estimation in Functional Mock-up Units. In Michael Tiller, Hubertus Tummescheit, and Luigi Vanfretti, editors, *Proceedings of the 1st American Modelica Conference*, pages 121–130. Modelica Association and Linköping University Electronic Press, 10 2018.
- [25] Hao Huang, Lei Chen, and Eric Hu. Model predictive control for energy-efficient buildings: An airport terminal building study. *IEEE International Conference on Control and Automation, ICCA, Taichung, Taiwan*, pages 1025–1030, 06 2014.
- [26] D. Picard, J. Drgoňa, M. Kvasnica, and L. Helsen. Impact of the controller model complexity on model predictive control performance for buildings. *Energy and Buildings*, 152:739 – 751, 2017.

- [27] Krzysztof Arendt, Muhyiddine Jradi, Hamid Reza Shaker, and Christian Veje. Comparative analysis of white-, gray- and black-box models for thermal simulation of indoor environment: Teaching building case study. In *Proceedings of the 2018 Building Performance Modeling Conference and SimBuild co-organized by ASHRAE and IBPSA-USA*, pages 173–180. ASHRAE, 9 2018.
- [28] Charles Corbin, Gregor Henze, and Peter May-Ostendorp. A model predictive control optimization environment for real-time commercial building application. *Journal of Building Performance Simulation*, 2012, 01 2012.
- [29] F. Jorissen, W. Boydens, and L. Helsens. TACO, an automated toolchain for model predictive control of building systems: implementation and verification. *Journal of Building Performance Simulation*, pages 180–192, 2018.
- [30] Martin Rätz, Amir Pasha Javadi, Marc Baranski, Konstantin Finkbeiner, and Dirk Müller. Automated data-driven modeling of building energy systems via machine learning algorithms. *Energy and Buildings*, 202:109384, 2019.
- [31] Zhong Guo, Austin R. Coffman, Jeffrey Munk, Piljae Im, Teja Kuruganti, and Prabir Barooah. Aggregation and data driven identification of building thermal dynamic model and unmeasured disturbance. *Energy and Buildings*, page 110500, 2020.
- [32] Anjukan Kathirgamanathan, Mattia De Rosa, Eleni Mangina, and Donal P. Finn. Data-driven predictive control for unlocking building energy flexibility: A review. *Renewable and Sustainable Energy Reviews*, 135:110120, 2021.
- [33] Samuel Prívarva, Jiří Cigler, Zdeněk Váňa, Frauke Oldewurtel, and Eva Žáčková. Use of partial least squares within the control relevant identification for buildings. *Control Engineering Practice*, 21(1):113 – 121, 2013.
- [34] Glenn Reynders, Jan Diriken, and Dirk Saelens. Quality of grey-box models and identified parameters as function of the accuracy of input and observation signals. *Energy and Buildings*, 82:263–274, 2014.
- [35] T. Zakula, P.R. Armstrong, and L. Norford. Modeling environment for model predictive control of buildings. *Energy and Buildings*, 85:549 – 559, 2014.
- [36] R.B. Gopaluni, R.S. Patwardhan, and S.L. Shah. Mpc relevant identification—tuning the noise model. *Journal of Process Control*, 14(6):699 – 714, 2004.
- [37] D. Laurí, M. Martínez, J.V. Salcedo, and J. Sanchis. Pls-based model predictive control relevant identification: Pls-ph algorithm. *Chemometrics and Intelligent Laboratory Systems*, 100(2):118 – 126, 2010.
- [38] A. Jain, F. Smarra, and R. Mangharam. Data predictive control using regression trees and ensemble learning. In *2017 IEEE 56th Annual Conference on Decision and Control (CDC)*, pages 4446–4451, Dec 2017.
- [39] Andrew Kusiak and Guanglin Xu. Modeling and optimization of HVAC systems using a dynamic neural network. *Energy*, 42(1):241 – 250, 2012. 8th World Energy System Conference, WESC 2010.
- [40] AE Ruano, EM Crispim, EZE Conceicao, and MMJR Lucio. Prediction of building’s temperature using neural networks models. *Energy and Buildings*, 38(6):682–694, 2006.
- [41] Hao Huang, Lei Chen, and Eric Hu. A neural network-based multi-zone modelling approach for predictive control system design in commercial buildings. *Energy and Buildings*, 97:86 – 97, 2015.
- [42] Klaus Kaae Andersen, Henrik Madsen, and Lars H. Hansen. Modelling the heat dynamics of a building using stochastic differential equations. *Energy and Buildings*, 31(1):13 – 24, 2000.
- [43] Peder Bacher and Henrik Madsen. Identifying suitable models for the heat dynamics of buildings. *Energy and Buildings*, 43(7):1511 – 1522, 2011.
- [44] R. De Coninck, F. Magnusson, J. Åkesson, and L. Helsens. Toolbox for development and validation of grey-box building models for forecasting and control. *Journal of Building Performance Simulation*, 9(3):288–303, 2016.
- [45] Abhinandana Boodi, Karim Beddiar, Malek Benamour, Yassine Amirat, and Mohamed Benbouzid. Intelligent systems for building energy and occupant comfort optimization: A state of the art review and recommendations. *Energies*, 11(10), 2018.
- [46] Tianbao Yang. Advancing non-convex and constrained learning: Challenges and opportunities. *AI Matters*, 5(3):29–39, December 2019.
- [47] Deepak Pathak, Philipp Krähenbühl, and Trevor Darrell. Constrained convolutional neural networks for weakly supervised segmentation. *CoRR*, abs/1506.03648, 2015.

- [48] Z. Jia, X. Huang, E. I. Chang, and Y. Xu. Constrained deep weak supervision for histopathology image segmentation. *IEEE Transactions on Medical Imaging*, 36(11):2376–2388, 2017.
- [49] C. K. Goh, Y. Liu, and A. W. K. Kong. A constrained deep neural network for ordinal regression. In *2018 IEEE/CVF Conference on Computer Vision and Pattern Recognition*, pages 831–839, 2018.
- [50] Pablo Márquez-Neila, Mathieu Salzmann, and Pascal Fua. Imposing hard constraints on deep networks: Promises and limitations. *CoRR*, abs/1706.02025, 2017.
- [51] Hoel Kervadec, Jose Dolz, Jing Yuan, Christian Desrosiers, Eric Granger, and Ismail Ben Ayed. Log-barrier constrained cnns. *CoRR*, abs/1904.04205, 2019.
- [52] Johannes Hendriks, Carl Jidling, Adrian Wills, and Thomas Schön. Linearly constrained neural networks. *Submitted to IEEE Transactions on Neural Networks and Learning Systems*, 2020.
- [53] Sam Greydanus, Misko Dzamba, and Jason Yosinski. Hamiltonian neural networks. *CoRR*, abs/1906.01563, 2019.
- [54] Michael Lutter, Christian Ritter, and Jan Peters. Deep lagrangian networks: Using physics as model prior for deep learning. *CoRR*, abs/1907.04490, 2019.
- [55] Rahul G. Krishnan, Uri Shalit, and David Sontag. Structured inference networks for nonlinear state space models. *AAAI*, 2016.
- [56] Danijar Hafner, Timothy P. Lillicrap, Ian Fischer, Ruben Villegas, David Ha, Honglak Lee, and James Davidson. Learning latent dynamics for planning from pixels. *CoRR*, abs/1811.04551, 2018.
- [57] D. Masti and A. Bemporad. Learning nonlinear state-space models using deep autoencoders. In *2018 IEEE Conference on Decision and Control (CDC)*, pages 3862–3867, 2018.
- [58] Syama S. Rangapuram, Matthias W. Seeger, Jan Gasthaus, Lorenzo Stella, Yuyang Wang, and Tim Januschowski. Deep state space models for time series forecasting. In S. Bengio, H. Wallach, H. Larochelle, K. Grauman, N. Cesa-Bianchi, and R. Garnett, editors, *Advances in Neural Information Processing Systems 31*, pages 7785–7794. Curran Associates, Inc., 2018.
- [59] Olalekan P. Ogunmolu, Xuejun Gu, Steve B. Jiang, and Nicholas R. Gans. Nonlinear systems identification using deep dynamic neural networks. *CoRR*, abs/1610.01439, 2016.
- [60] Tian Qi Chen, Yulia Rubanova, Jesse Bettencourt, and David K Duvenaud. Neural ordinary differential equations. In S. Bengio, H. Wallach, H. Larochelle, K. Grauman, N. Cesa-Bianchi, and R. Garnett, editors, *Advances in Neural Information Processing Systems 31*, pages 6571–6583. Curran Associates, Inc., 2018.
- [61] Lu Lu, Xuhui Meng, Zhiping Mao, and George E. Karniadakis. DeepXDE: A deep learning library for solving differential equations. *CoRR*, abs/1907.04502, 2019.
- [62] Kaiming He, Xiangyu Zhang, Shaoqing Ren, and Jian Sun. Deep residual learning for image recognition. *CoRR*, abs/1512.03385, 2015.
- [63] Eldad Haber and Lars Ruthotto. Stable architectures for deep neural networks. *CoRR*, abs/1705.03341, 2017.
- [64] Eldad Haber, Keegan Lensink, Eran Treister, and Lars Ruthotto. IMEXnet: A forward stable deep neural network. *CoRR*, abs/1903.02639, 2019.
- [65] J. Zico Kolter and Gaurav Manek. Learning stable deep dynamics models. In H. Wallach, H. Larochelle, A. Beygelzimer, F. d'Alché-Buc, E. Fox, and R. Garnett, editors, *Advances in Neural Information Processing Systems 32*, pages 11126–11134. Curran Associates, Inc., 2019.
- [66] Aaron Tuor, Jan Drgona, and Draguna Vrăbie. Constrained neural ordinary differential equations with stability guarantees. *arXiv preprint arXiv:2004.10883*, 2020.
- [67] Jan Drgona, Aaron Tuor, and Draguna Vrăbie. Constrained physics-informed deep learning for stable system identification and control of unknown linear systems. 2020.
- [68] Javier Rubio-Herrero, Vikas Chandan, Charles Siegel, Abhinav Vishnu, and Draguna Vrăbie. A learning framework for control-oriented modeling of buildings. In *2017 16th IEEE International Conference on Machine Learning and Applications (ICMLA)*, pages 473–478. IEEE, 2017.

- [69] Adam Paszke, Sam Gross, Francisco Massa, Adam Lerer, James Bradbury, Gregory Chanan, Trevor Killeen, Zeming Lin, Natalia Gimelshein, Luca Antiga, et al. Pytorch: An imperative style, high-performance deep learning library. In *Advances in Neural Information Processing Systems*, pages 8024–8035, 2019.
- [70] Diederik P Kingma and Jimmy Ba. Adam: A method for stochastic optimization. *arXiv preprint arXiv:1412.6980*, 2014.
- [71] Dan Hendrycks and Kevin Gimpel. Bridging nonlinearities and stochastic regularizers with gaussian error linear units. *CoRR*, abs/1606.08415, 2016.
- [72] Alice Mugnini, Gianluca Coccia, Fabio Polonara, and Alessia Arteconi. Performance assessment of data-driven and physical-based models to predict building energy demand in model predictive controls. *Energies*, 13(12), 2020.
- [73] Damien Picard, Maarten Sourbron, Filip Jorissen, Jiri Cigler, Lukás Ferkl, and Lieve Helsen. Comparison of model predictive control performance using grey-box and white-box controller models. In *Proceedings of the 4th International High Performance Buildings Conference, West Lafayette, IN, USA*, pages 1–10, West-Lafayette, Indiana, USA, 2016.
- [74] Razvan Pascanu, Tomas Mikolov, and Yoshua Bengio. Understanding the exploding gradient problem. *CoRR*, abs/1211.5063, 2012.
- [75] J. F. Kolen and S. C. Kremer. *Gradient Flow in Recurrent Nets: The Difficulty of Learning LongTerm Dependencies*, pages 237–243. 2001.
- [76] P. Schmid. Dynamic mode decomposition of numerical and experimental data. *Journal of Fluid Mechanics*, 656:5–28, 2008.
- [77] Jonathan H. Tu, Clarence W. Rowley, Dirk M. Luchtenburg, Steven L. Brunton, and J. Nathan Kutz. On dynamic mode decomposition: Theory and applications. *Journal of Computational Dynamics*, 1(2158-2491), 2014.